Fronts and Convective Cold Pools in the Oklahoma Mesonet. Part I: 15-Year Climatology

Andrew T. Lesage[*] and Steven K. Krueger

Department of Atmospheric Sciences, University of Utah, Salt Lake City, Utah

[*]*Corresponding author address:* Andrew T. Lesage, Department of Atmospheric Sciences, 135 S 1460 E, Rm 819, Salt Lake City, Utah 84112-0110.

E-mail: andy.lesage@utah.edu

ABSTRACT

The Oklahoma Mesonet provides an extensive surface observation network for analyzing frontal passages and convective cold pools. Frontal passages and convective cold pools were identified from Mesonet station time series of temperature and pressure as well as divergence on a triangular grid. From this, a 15-year climatology of frontal passages and convective cold pools was produced. Fronts and cold pools were characterized by their associated temperature drop, $-\Delta T$, and pressure rise, Δp. Winter had the largest $-\Delta T$ and Δp while spring had the lowest magnitudes of $-\Delta T$ and summer had the lowest magnitudes of Δp. Correlations between $-\Delta T$ and Δp were lowest in the more convectively active summer season. Surface convergence was similar ahead of fronts from spring to fall while surface divergence behind fronts exhibited a distinct seasonal cycle; the largest values occurred during the summer and the smallest during winter. The magnitude of convergence ahead of fronts was not a strong indicator of cold pool formation. Fronts and cold pools most likely occurred in spring and summer with summer having the highest percentage of fronts associated with cold pools. Fronts and cold pools were substantially more likely to occur during the late afternoon and early evening in the summer; other seasons showed a weak diurnal cycle with a slight nocturnal maximum. Western Oklahoma had higher frequencies of frontal passages and cold pools than Eastern Oklahoma. These findings could aid modeling studies in understanding cold pool processes and parameterizations.

1. Introduction

A convective cold pool is a region of cold air adjacent to the surface in a convective system. The cooling is due to evaporating precipitation in the system and can be influenced by downdrafts; however, downdrafts are not a necessary component. A surface pressure rise is expected in the cold pool as a result of the hydrostatic adjustment to cooling.

Cold pools are a prominent and common feature of convective systems which have been studied for over half a century. Observations from the Thunderstorm Project described regions of descending air behind a squall line caused by evaporative cooling (Newton 1950). Convergence ahead of the leading edge of the cold pool with divergence behind was also noted as a prominent feature in case studies of these squall lines. The results were similar to those observed during the Cloud Physics Project in which pressure jumps, temperature falls, wind shifts, and precipitation features were observed with squall lines (Tepper 1950). Tepper referred to the squall lines as propagating “pressure jump lines”.

In his synoptic analysis of squall lines in the Central United States, Fujita identified three main features of the associated surface pressure field: the pressure surge line, the thunderstorm high, and the wake depression (Fujita 1955). The pressure surge line marks the thunderstorms’ leading edge and moves in the storm propagation direction. The thunderstorm high, later more commonly known as a mesohigh, is the high pressure region led by the pressure surge line that contains cool downdrafts that spread out upon reaching the surface. The region of surface cooling from these downdrafts is what would become known as the cold pool of the thunderstorm and is often associated with the mesohigh. The wake depression is a region of low pressure, typically behind the thunderstorm high, which forms a “pressure dipole” with the thunderstorm high.

A gust front is “the leading edge of a mesoscale pressure dome followed by a surge of gusty winds on or near the ground” (Wakimoto 1982). These gust fronts often tilt forward with height due to surface drag effects (Markowski and Richardson 2012). The gust front propagation speed increases with the horizontal pressure gradient driving the gust front (Seigel and van den Heever 2012).

Cold pools have a large range of sizes. Those associated with a single cumulonimbus cell are on the order of 10 km across (Tompkins 2001) while cold pools associated with a mesoscale convective system (MCS) can be 100-400 km wide (Stensrud et al. 1999). In the Tompkins study the simulated cold pools had a mean lifetime of 2.5 hours, while in an observational study they lasted over 6 hours (Young et al. 1995). Air entrained from above the boundary layer into the wake of the downdraft resulted in recovery of the cold pools in the Tompkins study.

A four-stage convective life cycle for MCSs was developed by Engerer et al. (2008) based on Oklahoma Mesonet cases that produced cold pools: 1) first storms, 2) MCS initiation, 3) mature MCS, and 4) MCS dissipation. A mean potential temperature decrease of 9.5 K and a mean pressure increase of 3.2 hPa were found for cold pools during the first storms life cycle stage. The temperature deficit decreased to 5.4 K by the dissipating stage, but the pressure rise increased to 4.5 hPa for the mature stage before dropping to 3.3 hPa for the dissipation stage.

Adams-Selin and Johnson (2010) used Oklahoma Mesonet data to find dozens of bow echo cases. They produced a conceptual model for bow echoes that exhibits a pressure rise and temperature drop pattern associated with cold pools that is similar to those for MCSs.

Cold pool climatologies have been performed for the Atlas Mountains regions of North Africa (Emmel et al. 2010; Redl et al. 2015). For An Integrated Approach to the Efficient Management of Scarce Water Resources in West Africa (IMPETUS) data Emmel et al. (2010) used dew point temperature increases and wind speed thresholds for rain-free stations to identify density currents at stations. IR satellite images were examined manually to subjectively verify the presence of those identified density currents. Later work by Redl et al. (2015) used brightness temperature at microwave frequencies as an objective satellite verification method for cold pool leading edges.

In this study, the pressure and temperature changes over 5-minute intervals at surface Oklahoma Mesonet stations are analyzed for the 1997-2011 period to generate a dataset for a climatology. Individual station time series are used because the 5-minute temporal resolution is preferred compared to the roughly 40-km spatial resolution of the Oklahoma Mesonet grid as a means of detecting fronts and cold pools.

Surface divergence is another feature associated with dynamically active cold pools. In this study, cold pool area is defined to include regions of "strong" surface divergence following a frontal passage, which is detected by a temperature drop and a pressure rise. This definition of a cold pool is more restrictive than those used in other studies of cold pools which might include all areas with precipitation or maintain a cold pool until its temperature has recovered. As a result, cold pools in this study are generally smaller and shorter lasting. The cold pools defined here represent regions of active mesoscale cold air production due to precipitation evaporation. Other parts of a system not defined as a cold pool in this study but likely to be marked as a cold pool in other studies may be considered to be in a dissipating or residual cold pool.

Section 2 covers the methodology used in the frontal passage and cold pool analyses. Section 3 presents the results from the 15-year climatology of frontal passages and cold pools. The climatology includes the changes in temperature and pressure, the convergence/divergence associated with frontal passages, and the seasonal, diurnal, and geographic distribution of frontal passages and cold pools. Section 4 discusses the conclusions.

2. Methodology

a. Oklahoma Mesonet Dataset

The Oklahoma Mesonet dataset was used in this analysis (Brock et al. 1995; McPherson et al. 2007). The University of Oklahoma and Oklahoma State University are sponsors of the Oklahoma Mesonet. Mesonet observations have been collected since 1994 at 5-minute frequency. Each county of Oklahoma is represented by at least one station, for a total of over 100 stations. These stations are spaced roughly 40 km apart. The 1997-2011 period was selected for study (Atmospheric Radiation Measurement (ARM) Climate Research Facility 1970, updated hourly.).

Over the years stations have been added but for the purposes of this analysis, only the 113 stations present at the beginning of 1997 were considered. Of these, six were excluded due to residing in the Oklahoma panhandle. Of the remaining stations, each station was used for the years in which observation data for 1.5-m air temperature, 10-m vector average wind magnitude, 10-m vector average wind direction, and station pressure exists for at least 90% of the year. Between 99 and 104 of the 108 non-panhandle stations met the observation threshold each year.

The station resolution of the Oklahoma Mesonet is suitable to resolve large MCS events and their associated cold pools. Smaller systems, such as a cold pool from an individual cumulonimbus cloud, might be missed in the Mesonet data.

b. Mesonet Grid

Mesonet stations that met the observation threshold described in section 2a for a year were gridded using the Delaunay triangulation procedure (Figure 1). Triangular grid cells were defined in order to calculate surface divergence (described in section 2c). The resulting grids for each year contained some low aspect ratio triangles[1] along the border which were removed. Two stations very close to each other located at approximately 35°N 98°W resulted in two low aspect ratio triangles which were also removed. The station coordinates (longitude, latitude, and altitude) changed in the case of a few stations which moved during the 15-year period (1997-2011). These stations were excluded from the grid during the year in which they moved. Due to the varying number of stations that met the observation threshold each year, and to stations that changed location during a year, the grid was adjusted slightly from year to year.

It was also determined that triangles with relatively long side lengths were not representative of the temporal scales used in the analysis of this study, so all triangles with a longest side length of greater than 80 km were excluded. This resulted in the removal of 10 to 13 triangles each year which were primarily along the borders.

c. Divergence

The Mesonet stations' 5-minute average wind magnitude and direction values were used to determine the divergence in each Mesonet triangle. This calculation used the equations for the horizontal divergence of triangles on irregular grids (Davies-Jones 1993; Dubois and Spencer 2005). Sun and Krueger (2012) performed these divergence calculations for the Oklahoma Mesonet specifically for surface divergence analyses. The divergence values then had a 15-minute rolling average applied to smooth out timing discrepancies that may occur in a study with large station spacing.

d. Front Analysis

This study looked at frontal passages as potential indicators for cold pool existence. Previous studies have shown that temperature falls and pressure rises are associated with gust fronts and cold

[1]The aspect ratio of a triangle is defined as $2R_i/R_o$ where R_i is the radius of the circle inscribed within a triangle and R_o is the radius of the circle circumscribed around the triangle.

pools (Engerer et al. 2008; Adams-Selin and Johnson 2010). These temperature falls and pressure rises were used to mark the frontal passage. In addition to fronts associated with convective and mesoscale systems, some synoptic fronts were also detected in the front analysis.

Temperatures at each station were adjusted to remove the diurnal cycle. The diurnal cycle for a station was calculated based on the average temperature for each observation time. An example of an observation time is 10 June 1200 UTC. The average temperature was determined by using all valid temperature measurements at a station during the 15-year period for the observation time as well as all of the observations 24 and 48 hours before and after the observation time at the station (Eq. 1).

$$T_{\text{diur.}} = [\sum_{1997}^{2011} \sum_{\text{day}-2}^{\text{day}+2} T_t]/n \tag{1}$$

In this equation, n is the total number of valid observations and t is the observation time. Without the removal of the diurnal cycle, many spurious frontal passages would be generated by the analysis in the late afternoon and evening when the surface is rapidly cooling. Similarly, the diurnal cycle was also calculated for the pressure observations (Eq. 2).

$$P_{\text{diur.}} = [\sum_{1997}^{2011} \sum_{\text{day}-2}^{\text{day}+2} P_t]/n \tag{2}$$

Temperature and pressure measurements were also adjusted to account for elevation. Each station was adjusted to the Mesonet-averaged station elevation (between 365 and 370 m depending on the year; only stations that met the observation threshold for the particular year were included in the average altitude for that year). The temperature values were adjusted to the mean station elevation by changing the station values dry adiabatically, while the pressure values were adjusted using the hypsometric equation. The elevation adjustments had little impact on the analyses since the differences in adjustment from one observation time to the next were very small.

Since temperature drops and pressure rises comprise the core aspects of gust fronts and cold pools, combining these two variables provides a useful metric for front occurrence and strength. The front score (FS) is a unitless variable used in this study to represent the strength of a frontal passage. The FS uses the diurnal- and elevation-adjusted over 30-minute intervals, temperature falls, $-(\Delta T)_{30}$, and pressure rises, $(\Delta p)_{30}$, calculated every 5 minutes. For example, the FS at 1230 UTC uses the changes in adjusted temperature and pressure between 1200 UTC and 1230 UTC. A 1 hPa pressure increase is equivalent to a 1 K temperature drop. Later, observations will show that temperature drops tend to be larger than pressure rises. However, temperature has often been used as a cold pool initiation or ending signal so it is allowed the higher relative weight here. Adding these changes yields the FS:

$$\mathrm{FS}(t) = -1\ \mathrm{K}^{-1}(\Delta T)_{30} + 1\ \mathrm{hPa}^{-1}(\Delta p)_{30}. \tag{3}$$

As an example, the FSs at the Blackwell Mesonet station for JJA 1997 are shown in Figure 2.

FSs were used to detect when a frontal passage occurred at a Mesonet station or triangle. A front is considered to have reached a Mesonet station when (1) the FS at the station exceeds a threshold and (2) the FS is the maximum value reached during the 6 hours centered at the analysis time. Requiring both conditions more accurately identifies the primary front associated with a system. FSs of 3 and 5 were used as the thresholds for "fronts" and "strong fronts," respectively.

A frontal passage at a Mesonet triangle (as opposed to a Mesonet station) is stipulated to have occurred if all three stations that comprise the triangle corners experience a frontal passage within a 2-hour interval. The 2-hour limit was the reason for limiting maximum triangle side length to 80 km since slower fronts would be less likely to be detected in larger triangles leading to an underestimate in frontal passage frequency. However, extending the 2-hour limit would have captured more spurious fronts. The duration of a frontal passage at a triangle is the time elapsed from when the first corner is reached until the time when the last corner is reached. The resulting fronts could be tracked across the Mesonet as they progress through Oklahoma.

e. Cold Pool Analysis

The front analysis was necessary for determining the location of potential cold pools since a gust front marks the leading edge of a cold pool (Wakimoto 1982). Cold pools are primarily identified by temperature falls and pressure rises, as was the case for the frontal passages in the previous section. Additionally, "active" cold pools are regions of surface divergence. Surface divergence is an identifier used in this study to separate fronts associated with active cold pools from other frontal passages. Consequently, *a cold pool region is defined in this study to be a Mesonet triangle with surface divergence (that exceeds a threshold described below) following a frontal passage*.

This definition is more limiting than those that are generally used for which continuing precipitation and/or a lack of surface temperature recovery indicates a sustained cold pool. The cold pools in this study consist of regions in which a cold air mass is expanding via precipitation processes such as evaporative cooling and downdrafts whereas other studies include areas in which cold air persists due to a lack of surface heating. Precipitation is necessary for evaporative cooling, though the precipitation does not have to reach the ground for evaporative cooling to occur. Dry (non-precipitating) frontal passages generally did not result in cold pools in this study due to insufficiently large divergence values.

Quantitatively, a cold pool was deemed to have occurred in this study at a Mesonet triangle if the triangle experienced a frontal passage and if the 15-minute-averaged strong divergence threshold ($10^{-4}\mathrm{s}^{-1}$) was exceeded within half an hour before to an hour after the front propagates halfway through the triangle. The longer time duration after the frontal passage recognizes that cold pools follow gust fronts. It is possible, given the resolution of the Mesonet grid, that a cold pool region could seemingly be slightly ahead of a front which would suggest a strong cold pool covering less than half the triangle area. When a cold pool region is determined to have occurred, its duration at the triangle is calculated. The time interval during which the divergence exceeds half of its maximum value in a triangle is defined as the stations' cold pool duration. Fronts and cold pool regions can be tracked across the Mesonet giving a detailed view of the analysis for case studies and cold pool areas which is explored in Part II.

3. 15-year Climatology of Fronts and Cold Pools

The 1997-2011 period of Oklahoma Mesonet data was analyzed for frontal passages (across Mesonet triangles) and cold pools and statistics were compiled. These frontal passage and cold pool statistics are now presented for: (1) temperature and pressure changes, (2) convergence/divergence, (3) seasonal distribution, (4) diurnal distribution, and (5) geographic distribution.

a. Temperature and Pressure Changes

For each frontal passage across a Mesonet triangle, all three corner stations of the triangle were individually included in the statistics of changes in temperature and pressure. The temperature and pressure changes during all frontal passages (FS 3+), and strong frontal passages (FS 5+) are shown in Figure 3.

The maximum temperature drop during a frontal passage, $-\Delta T$, was calculated by subtracting the lowest temperature within 2 hours after the frontal passage at a station from the highest temperature within 30 minutes before the frontal passage. The maximum pressure rise, Δp, was calculated by subtracting the lowest pressure within 30 minutes before the frontal passage at a station from the highest pressure within 2 hours after the frontal passage.

Generally, results for all frontal passages were similar to those for fronts associated with cold pools (not shown). The magnitudes of both $-\Delta T$ and Δp were slightly greater on average for fronts with cold pools compared to all fronts (FS 3+). For strong fronts (FS 5+) the converse is the case, with strong fronts yielding slightly greater magnitudes of average $-\Delta T$ and Δp than strong fronts resulting in cold pools.

Average temperature drops during frontal passages were lower in magnitude in spring and higher in magnitude in winter. Average pressure rises had a distinct minimum in magnitude in summer while the winter pressure changes were largest on average.

Engerer et al. (2008) analyzed 1389 Oklahoma Mesonet station time series to determine pressure and temperature changes associated with convective cold pools during each of the four MCS life stages. The MCS events were chosen because they had leading convective lines of 200 km or more in length sometime during their life cycle. Their study found that the average pressure rise in cold pools from 39 MCS events between April and August was 4.5 hPa (which occurred during the mature stage) while the average temperature fall was 9.5 K (first storms stage). Their weighted average pressure rise was 4.1 hPa and weighted average temperature fall was 6.9 K. The ratio $-\Delta T/\Delta p$ calculated from Engerer et al.'s results decreases from 3.0 for first storms to 1.6 for mature and dissipating storms while the ratio of the weighted averages of $-\Delta T$ and Δp was 1.7.

Since the 15-year climatology was generated from Mesonet triangles which may only see part of a storm lifecycle for a given event, it is better to compare to the weighted average of Engerer et al.'s results. The seasonal averages for strong fronts resulting in cold pools in the 15-year climatology were 3.5 hPa pressure rises in spring, 2.5 hPa pressure rises in summer, 7.5 K temperature falls in spring, and 7.7 K temperature falls in summer, with $-\Delta T/\Delta p$ ratios of 2.1 for spring and 3.1 for summer. Some of the difference between the 15-year climatology and Engerer et al.'s results is likely a result of the 15-year climatology including more than just MCS events.

For individual stations, a frontal passage typically exhibited a 3 to 9 K temperature drop and a 0 to 4 hPa pressure rise (Figure 4). The correlation between $-\Delta T$ and Δp was low (0.28). Correlations were calculated for all fronts and strong fronts for each season (Figure 5). The correlations did not change significantly when only strong fronts were considered. Likewise, considering only fronts resulting in cold pools made little change in the correlations (not shown). Summer correlations were the smallest in magnitude while winter and spring had the largest correlations.

The correlations of $-\Delta T$ with Δp varied from 0.44 for strong fronts during the spring to only 0.06 for strong fronts during the summer. Engerer et al. (2008) also reported a weak to moderate correlation (0.38) between $-\Delta T$ with Δp, noting that for Δp between 4 and 6 hPa, $-\Delta T$ can vary by more than a factor of 10. Engerer et al. (2008) speculated that the weak relationship between $-\Delta T$ and Δp is due to the complex vertical buoyancy profiles that often occur within and above cold pools (Bryan et al. 2005). As a consequence, the surface temperature deficit is often not correlated with the buoyancy profile and the resulting surface pressure rise. This relationship between $-\Delta T$ and Δp may at least partially explain the low correlations found during the summer, which was when the largest fraction of fronts were associated with cold pools (detailed in section 3c).

b. Convergence/Divergence

Divergence values were calculated for the beginning, middle, and end of each triangles' frontal passages. The beginning of the frontal passage was defined as the observation time when the first corner of a Mesonet triangle experiences a local maximum FS. The end of the frontal passage was defined as the observation time when the third corner of a Mesonet triangle experiences a local maximum FS. The middle of the frontal passage was the observation time halfway between the beginning and the end.

The average divergence values for all frontal passages are shown (Figure 6). On average, as a front reaches a Mesonet triangle, there is strong convergence (divergence $< -10^{-4}$ s^{-1}). The magnitude of the convergence at the beginning varied slightly from season to season with convergence for all fronts slightly weaker in winter and convergence for strong fronts slightly stronger in spring and fall. During the middle of the frontal passages, there were large seasonal differences in divergence. Summer frontal passages had divergence on average while the other three seasons maintained convergence. At the end of a frontal passage, summer had the strongest divergence on average: a factor of 2 larger than spring and fall, and a factor of 5 larger than winter. This is largely attributable to the greater evaporative cooling in the summer compared to winter. End-of-front divergence in summer was roughly the same magnitude as beginning-of-front convergence. For the other three seasons the magnitude of convergence at the beginning of a frontal passage was 2 to 5 times the magnitude of divergence at the end of a frontal passage.

Average divergence values for frontal passages that produced cold pools are also shown (Figure 7). Because cold pools required the divergence threshold to be exceeded, their ending divergence and mid-passage divergence values were larger than for all frontal passages. However, the seasonal pattern was about the same as for frontal passages with summer having the highest divergence values for the middle and end of frontal passages and winter having the lowest convergence at the beginning of frontal passages and lowest divergence at the end of frontal passages. It is notable that the beginning covergence values were roughly the same for cold pools as for all frontal passages. This suggests that the strength of convergence ahead of a front is not closely related to the strength of divergence behind a front.

c. Seasonal Distributions

The seasonal distributions of frontal passages and cold pools were also determined. For these calculations, the data from the triangles that experienced fronts or cold pools were used (Figure 8). There were more cold pools during the summer than the other seasons while the number of frontal passages were similar for spring and summer. Winter had the lowest number of fronts and cold pools. The dominance of spring and summer matches up well with the time of the annual maximum of convective activity in Oklahoma. Frontal passages during the summer also had the highest percentage of fronts leading to cold pools. A greater fraction of strong fronts (FS 5+) compared to all fronts (FS 3+) resulted in cold pool formation.

One factor that influences the seasonal distributions of fronts and cold pools is the dependence of precipitation evaporation rate on temperature. An increase in temperature leads to an increase in precipitation evaporation rate, for the same relative humidity and rain water mixing ratio. As a result, summer months are more highly influenced by precipitation evaporation which explains some of the seasonal differences, particularly for cold pools. Additionally, seasonal variation between convective and stratiform precipitation is likely an influence in this result. During the summer, high precipitation rates occur more frequently than during the winter.

d. Diurnal Distributions

The mean diurnal distributions of frontal passages and cold pools were calculated by summing the number of fronts and cold pools present in all triangles for each hourly interval (0000-0055 UTC, 0100-0155 UTC,..., 2300-2355 UTC) during each season for the 15-year period of record (1997–2011) (Figure 9). Seasons were defined as: MAM for spring, JJA for summer, SON for fall, and DJF for winter. The error bars indicate the standard deviations of the yearly means.

There was a significant seasonal variation in the diurnal distribution of frontal passages. In the summer (Figure 9b) there was a large peak in frontal passage frequency in the afternoon, from 20-01 UTC (14-19 LST), with frontal passage frequencies then twice as high as during the rest of the day. The other three seasons exhibited relatively small amplitudes in their diurnal cycles. The diurnal distribution of cold pool frequency (not shown) was very similar to that for frontal passages.

The standard deviations shown in Figure 9 are quite large. Despite it being impossible for there to be more strong frontal passages than total fronts in a given year, the standard deviations overlap which means it can be expected that some years have more strong fronts in a given hour of the day for a season than other years have total fronts in that hour for a season.

The percentages of frontal passages with cold pools were also calculated for the diurnal cycle (Figure 10). For most hours of the day in each of the four seasons, the percentage of strong fronts with cold pools was higher than the percentage of all fronts with cold pools. Consistently throughout the year, the evening hours, 00-06 UTC (18-00 LST), had the largest spread between all and strong frontal passages associated with cold pools. In spring (Figure 10a) roughly 60% of fronts resulted in cold pools throughout most of the day. The morning hours were the exception with the percentage dropping below 50% for several hours (15-19 UTC). Summer (Figure 10b) had the largest fraction of frontal passages yielding cold pools, exceeding 90% in the evening hours for strong frontal passages. No individual hour during summer fell below 70% of total fronts yielding cold pools. In the fall evening hours (Figure 10c) 60% of frontal passages and 75% of strong frontal passages resulted in cold pools. During the day these percentages fell to between 40 and 55% until the mid-afternoon. In the winter (Figure 10d) the fraction of frontal passages which resulted in cold pools was uniform throughout the day between 30 and 40%, which was less than half as large as for summer.

e. Geographic Distribution

Finally, the geographic distributions of frontal passages and cold pools across the Mesonet were computed. It was found that Mesonet triangles with larger areas and larger longest side lengths had lower frequencies of frontal passages and cold pool occurrences on average. This was expected since all three triangle corners have to be crossed within two hours to qualify as a frontal passage for the triangle. Linear regressions were performed using a least-squares fit to determine the dependence of triangle frequencies on triangle area and longest side length. The regressions were calculated for all fronts, strong fronts, all cold pools, and cold pools with strong fronts.

The linear fits were assumed to exactly describe how the frontal passage and cold pool frequencies vary with (1) the triangle area, and (2) the longest side length, relative to the mean frontal passage or cold pool frequency of a triangle with an area equal to the Mesonet mean triangle area ($\sim$ 802 km^{-2}) and a longest side length equal to the Mesonet mean longest side length ($\sim$ 55 km). Any deviations of the observed frontal passage or cold pool frequency for a specific Mesonet triangle from those predicted by the linear fits for that triangles' area or side length were assumed to be due to geographical variability. The two deviation methods for each triangle were averaged and then added to the mean frontal passage or cold pool frequency. Before plotting, the adjusted frequencies were spatially smoothed using a three iteration Barnes analysis with a half-degree smoothing length scale. The end results shown are the geographic distributions of front frequencies (Figure 11) and cold pool frequencies (Figure 12).

For the frontal passage frequencies, a west to east gradient is apparent with western regions of Oklahoma exhibiting larger frequencies of frontal passages than eastern regions of Oklahoma (Figure 11a). Strong frontal passage frequencies (Figure 11b) have a similar distribution. In both cases the highest frequencies are in the northwest and the lowest frequencies in the southeast.

The geographic distribution of cold pool frequencies is similar to that for frontal passages (Figure 12a). Western areas have the highest cold pool frequencies while the northeast and southeast have the lowest average frequencies of cold pools. There is slightly more irregularity to the pattern for cold pools compared to that for fronts. Cold pools resulting from strong fronts (Figure 12b) show roughly the same geographic frequency pattern as for all cold pools.

One possible reason for the higher frequency of frontal passages in Western Oklahoma is the dryline which frequently develops in the lee of the Rocky Mountains and advances into Oklahoma where numerous case studies have been investigated over the years (McCarthy and Koch 1982; Ziegler and Hane 1993; Buban et al. 2007). The dryline is a favored zone for cumulus cloud formation and deep convection initiation. A climatology of springtime dryline position matches well with the frontal passage geographic distribution anomaly pattern (Hoch and Markowski 2005). Their Figure 2 shows that the dryline is most frequently located around 101°W longitude and the range is generally from 103°W to 97°W with rare occurrences farther eastward. The west to east pattern is slightly weaker for cold pools, possibly suggesting that western stations have a higher rate of frontal passages not resulting in cold pools.

4. Conclusions

A 15-year climatology of Oklahoma Mesonet frontal passages and convective cold pools was created and analyzed. Previous studies involving cold pools in the Oklahoma Mesonet have looked at shorter time periods with a focus on features such as MCSs (Engerer et al. 2008) and squall lines (Adams-Selin and Johnson 2010).

Frontal passages at Mesonet stations were objectively detected by calculating a non-dimensional variable, the front score (FS), from 30-minute temperature falls and pressure rises. When all three stations in a Mesonet triangle experienced a frontal passage within 2 hours, a front was deemed to have crossed the Mesonet triangle. A cold pool event required a frontal passage to occur at a Mesonet triangle and for the divergence of the triangle to exceed $10^{-4}\mathrm{s}^{-1}$ within half an hour before or an hour after the frontal passage was halfway through the triangle.

The temperature falls and pressure rises during frontal passages were objectively determined. Spring had the smallest average temperature falls while summer had the smallest average pressure rises. Both variables had their largest average magnitude changes in the winter. Correlations between $-\Delta T$ and Δp for individual frontal passages were low, 0.28, with the smallest correlation in summer and highest in winter and spring. This result indicated that there was a large variety in the vertical structure of the temperature perturbations accompanying cold pools. The average temperature and pressure changes and their correlations were generally similar for fronts with cold pools and for all fronts. Since the Mesonet observations are at the surface, obtaining vertical profiles of temperature could improve understanding of the reasons for the low correlations between changes in pressure and temperature during frontal passages, particularly in the summer.

Convective cold pools were evaluated based on temperature falls, pressure rises, and surface divergence. The associated gust front exhibits convergence ahead of the front and divergence behind the front. Convergence values ahead of frontal passages were similar from spring to fall with slightly lower values in winter. However, summer frontal passages transitioned to divergence sooner, and had larger divergence values as a front finished crossing a Mesonet triangle, than was the case for the other seasons, especially winter. While divergence values were much stronger for fronts resulting in cold pools than all fronts because of the divergence requirement, the convergence values ahead of a front showed very little difference between all fronts and fronts resulting in cold pools.

Seasonally, spring and summer had the highest frequency of frontal passages (approximately 9 total fronts including 3 strong fronts per Mesonet triangle per season), while summer had the highest frequency of cold pools and the percentage of frontal passages which resulted in cold pools (79% of fronts and 87% of strong fronts). Winter was lowest in all three categories with roughly half as many fronts, a quarter as many cold pools and only 35% of fronts and 40% of strong fronts resulting in cold pools.

The diurnal cycle of fronts and cold pools showed a strong seasonal variation. During the summer, frontal passages and cold pools were most frequent in the late afternoon to evening hours, coinciding with daytime-heating-induced convection, over twice as often as the other hours ($\sim$130 vs $\sim$50 per summer). The other seasons had much smaller diurnal variation in frontal passage and cold pool frequency. The summer pattern was the dominant influence on the annual pattern for the diurnal cycle.

Geographically, the size of Mesonet triangles, in terms of area and longest side length, had a significant influence on the analyzed frequency of frontal passages and cold pools. After this analysis artifact was accounted for, it was evident that western regions of Oklahoma experienced higher frequencies of frontal passages and cold pools than eastern regions.

The methods used in this analysis could be applied to simulations using convection-resolving models such as the Weather Research and Forecasting (WRF) model and the System for Atmospheric Modeling (SAM). Particularly useful would be increased resolution in a model relative to that of the Oklahoma Mesonet. Higher resolution would improve the sampling, especially for cases of smaller-scale features and isolated convection that can be missed by the 40-km spacing of the Mesonet stations. A regularly spaced grid in a model simulation would also aid in evaluating geographic distributions.

Pressure rise data in this study could serve as a basis for comparison of rain evaporation estimates. Fujita proposed a method to estimate rain evaporation which assumed that the pressure rise is a result of cooling (and associated hydrostatic adjustment) due to precipitation evaporation (Fujita 1959). Comparing such rain evaporation estimates to rain evaporation derived from convection-resolving model simulations would allow one to test and refine the method. The resulting rain evaporation estimates could be used to evaluate and improve microphysical parameterizations in convection-resolving models. More accurately representing regions of cold air production due to precipitation evaporation and surface outflow boundaries could lead to an improved predictability of cold pool properties and convection initiation which could, in turn, be used to evaluate cold pool parameterizations in global weather and climate models.

Acknowledgments. This research was supported by the Office of Science (BER), U.S. Department of Energy, Grant No. DE-FG02-08ER64553. Data were obtained from the Atmospheric Radiation Measurement (ARM) Program sponsored by the U.S. Department of Energy, Office of Science, Office of Biological and Environmental Research, Climate and Environmental Sciences Division. Oklahoma Mesonet data are from a cooperative venture between Oklahoma State University and The University of Oklahoma, supported by the taxpayers of Oklahoma.

References

Adams-Selin, R. D., and R. H. Johnson, 2010: Mesoscale surface pressure and temperature features associated with bow echoes. *Mon. Wea. Rev.*, **138**, 212–227, doi:10.1175/2009MWR2892.1.

Atmospheric Radiation Measurement (ARM) Climate Research Facility, 1970, updated hourly.: Oklahoma Mesonet (05OKM). 1997-01-01 to 2011-12-31. Southern Great Plains (SGP) External Data (satellites and others) (X1), Compiled by: Atmospheric Radiation Measurement (ARM) Climate Research Facility Data Archive: Oak Ridge, Tennessee, USA. Data set accessed 2012-02-06., www.arm.gov/data/datastreams/05okm.

Brock, F. V., K. C. Crawford, R. L. Elliott, G. W. Cuperus, S. J. Stadler, H. L. Johnson, and M. D. Eilts, 1995: The Oklahoma Mesonet: A technical overview. *J. Atmos. Oceanic. Technol.*, **12**, 5–19, doi:10.1175/1520-0426(1995)012⟨0005:TOMATO⟩2.0.CO;2.

Bryan, G. H., D. Ahijevych, C. Davis, S. Trier, and M. Weisman, 2005: Observations of cold pool properties in mesoscale convective systems during BAMEX. *Preprints, 11th Conf. on Mesoscale Processes*, Albuquerque, NM, Amer. Meteor. Soc., JP5J.12. [Available online at http://ams.confex.com/ams/pdfpapers/96718.pdf.].

Buban, M. S., C. L. Ziegler, E. N. Rasmussen, and Y. P. Richardson, 2007: The dryline on 22 May 2002 during IHOP: Ground-radar and in situ data analyses of the dryline and boundary layer evolution. *Mon. Wea. Rev.*, **135**, 2473–2505, doi:10.1175/MWR3453.1.

Davies-Jones, R., 1993: Useful formulas for computing divergence, vorticity, and their errors from three or more stations. *Mon. Wea. Rev.*, **121**, 1449–1458, doi:10.1175/1520-0493(1993)121⟨0713:UFFCDV⟩2.0.CO;2.

Dubois, J. A., and P. L. Spencer, 2005: Computing divergence from a surface network: Comparison of the triangle and pentagon methods. *Wea. Forecasting*, **20**, 596–608, doi:10.1175/WAF867.1.

Emmel, C., P. Knippertz, and O. Schulz, 2010: Climatology of convective density currents in the southern foothills of the Atlas Mountains. *J. Geophys. Res.*, **115**, D11 115, doi:10.1029/2009JD012863.

Engerer, N. A., D. J. Stensrud, and M. C. Coniglio, 2008: Surface characteristics of cold pools. *Mon. Wea. Rev.*, **136**, 4839–4849, doi:10.1175/2008MWR2528.1.

Fujita, T., 1955: Results of detailed synoptic studies of squall lines. *Tellus*, **7**, 405–436, doi:10.1111/j.2153-3490.1955.tb01181.x.

Fujita, T., 1959: Precipitation and cold air production in mesoscale thunderstorm systems. *J. Meteor.*, **16**, 454–466, doi:10.1175/1520-0469(1959)016⟨0454:PACAPI⟩2.0.CO;2.

Hoch, J., and P. M. Markowski, 2005: A climatology of springtime dryline position in the U.S. Great Plains region. *J. Climate*, **18**, 2132–2137, doi:10.1175/JCLI3392.1.

Markowski, P. M., and Y. P. Richardson, 2012: *Mesoscale Meteorology in Midlatitudes.* Wiley-Blackwell, 407 pp., doi:10.1002/9780470682104.

McCarthy, J., and S. E. Koch, 1982: The evolution of an Oklahoma dryline. Part I: A meso- and subsynoptic-scale analysis. *J. Atmos. Sci.*, **39**, 225–236, doi:10.1175/1520-0469(1982)039⟨0225:TEOAOD⟩2.0.CO;2.

McPherson, R. A., and Coauthors, 2007: Statewide monitoring of the mesoscale environment: A technical update on the Oklahoma Mesonet. *J. Atmos. Oceanic Technol.*, **24**, 301–321, doi:10.1175/JTECH1976.1.

Newton, C. W., 1950: Structure and mechanism of the prefrontal squall line. *J. Meteor.*, **7**, 210–222, doi:10.1175/1520-0469(1950)007⟨0210:SAMOTP⟩2.0.CO;2.

Redl, R., A. H. Fink, and P. Knippertz, 2015: An objective detection method for convective cold pool events and its application to Northern Africa. *Mon. Wea. Rev.*, **143**, 5055–5072, doi:10.1175/MWR-D-15-0223.1.

Seigel, R. B., and S. C. van den Heever, 2012: Simulated density currents beneath embedded stratified layers. *J. Atmos. Sci.*, **69**, 2192–2200, doi:10.1175/JAS-D-11-0255.1.

Stensrud, D. J., G. S. Manikin, E. Rogers, and K. E. Mitchell, 1999: Importance of cold pools to NCEP mesoscale Eta model forecasts. *Wea. Forecasting*, **14**, 650–670, doi:10.1175/1520-0434(1999)014⟨0650:IOCPTN⟩2.0.CO;2.

Sun, R., and S. K. Krueger, 2012: Mesoanalysis of the interactions of precipitating convection and the boundary layer. *J. Adv. Model. Earth Syst.*, **4**, M04 004, doi:10.1029/2011MS000096.

Tepper, M., 1950: A proposed mechanism of squall lines: The pressure jump line. *J. Meteor.*, **7**, 21–29, doi:10.1175/1520-0469(1950)007⟨0021:APMOSL⟩2.0.CO;2.

Tompkins, A. M., 2001: Organization of tropical convection in low vertical wind shears: The role of cold pools. *J. Atmos. Sci.*, **58**, 1650–1672, doi:10.1175/1520-0469(2001)058⟨1650:OOTCIL⟩2.0.CO;2.

Wakimoto, R. M., 1982: The life cycle of thunderstorm gust fronts as viewed with Doppler radar and rawinsonde data. *Mon. Wea. Rev.*, **110**, 1060–1082, doi:10.1175/1520-0493(1982)110⟨1060:TLCOTG⟩2.0.CO;2.

Young, G. S., S. M. Perugini, and C. W. Fairall, 1995: Convective wakes in the equatorial western Pacific during TOGA. *Mon. Wea. Rev.*, **123**, 110–123, doi:10.1175/1520-0493(1995)123⟨0110:CWITEW⟩2.0.CO;2.

Ziegler, C. L., and C. E. Hane, 1993: An observational study of the dryline. *Mon. Wea. Rev.*, **121**, 1134–1151, doi:10.1175/1520-0493(1993)121⟨1134:AOSOTD⟩2.0.CO;2.

LIST OF FIGURES

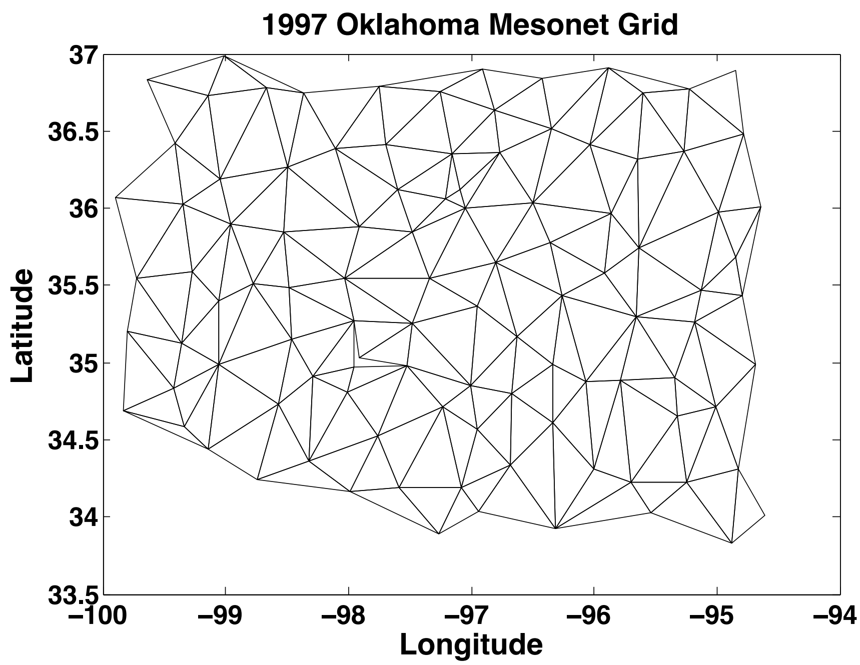

FIG. 1. Map of the Oklahoma Mesonet grid used for 1997. Delaunay triangulation was used to connect the stations to form the grid. Low aspect ratio triangles were removed. The triangles removed were primarily on the outer border with the exception of two near 35°N 98°W.

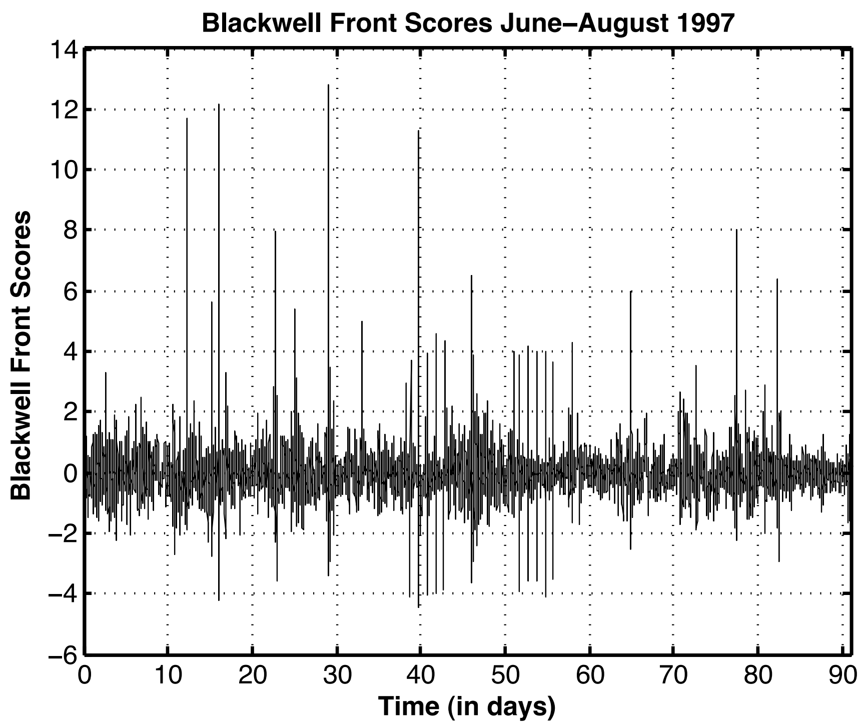

FIG. 2. Front scores for the JJA 1997 period at the Blackwell Mesonet station (36.75°N, 97.25°W). Large positive front scores indicate frontal passages.

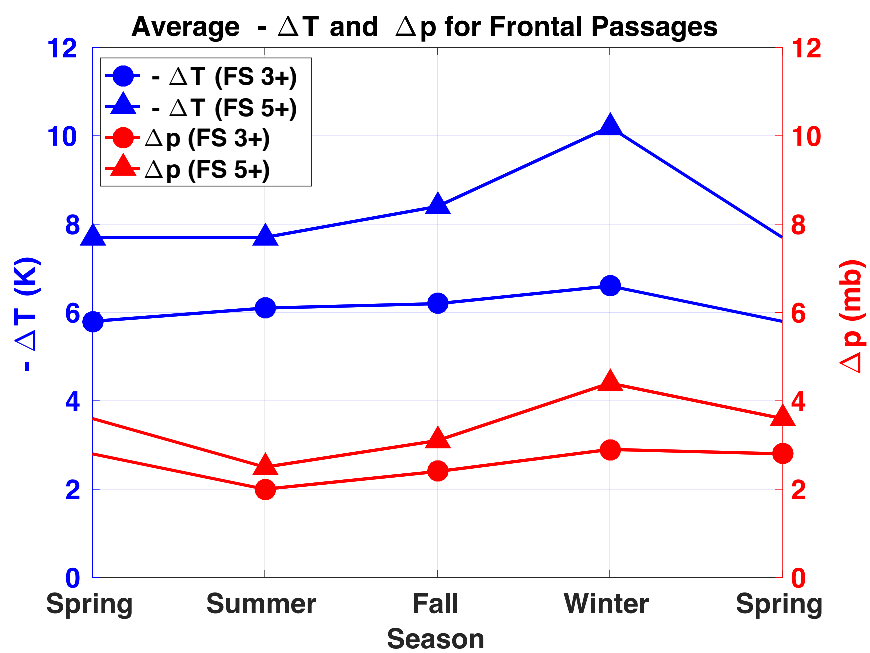

554 FIG. 3. Seasonal average $-\Delta T$ and Δp for all 1997-2011 frontal passages (FS 3+) and strong frontal passages
555 (FS 5+).

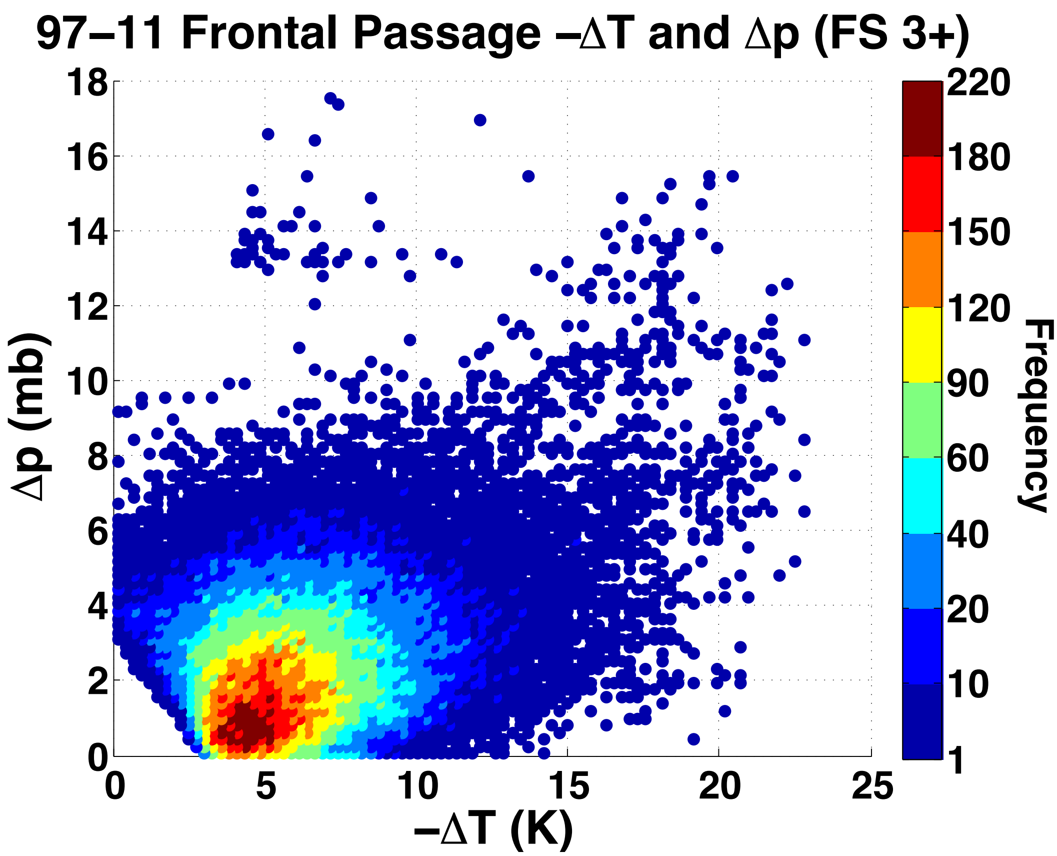

FIG. 4. Δp versus $-\Delta T$ at stations that are part of all frontal passages across triangles in the Oklahoma Mesonet from the 1997-2011 period. The color bar represents the frequency of occurrence. The correlation is 0.28.

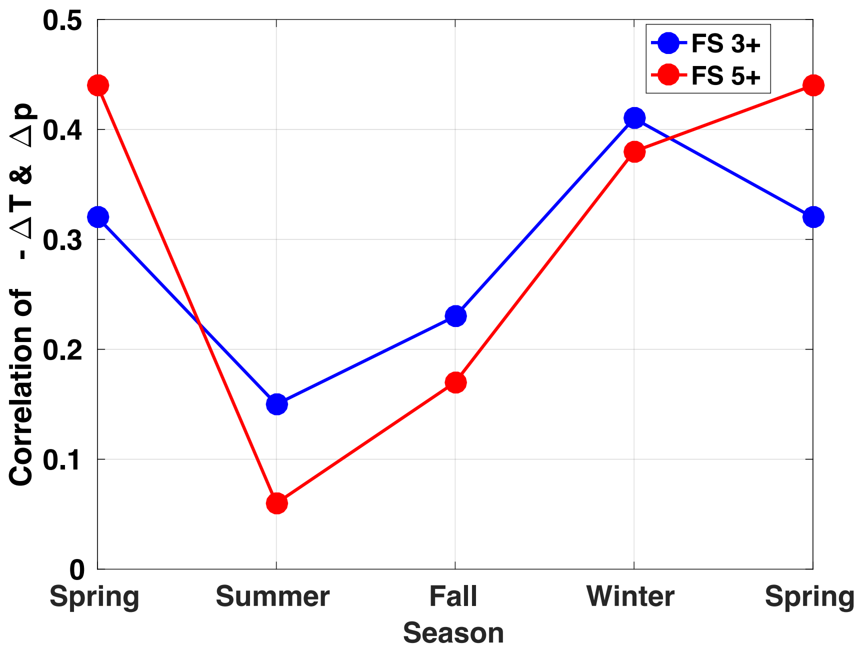

559 FIG. 5. Seasonal correlations between $-\Delta T$ and Δp at stations that were part of all frontal passages (FS 3+)
560 and strong frontal passages (FS 5+) across triangles.

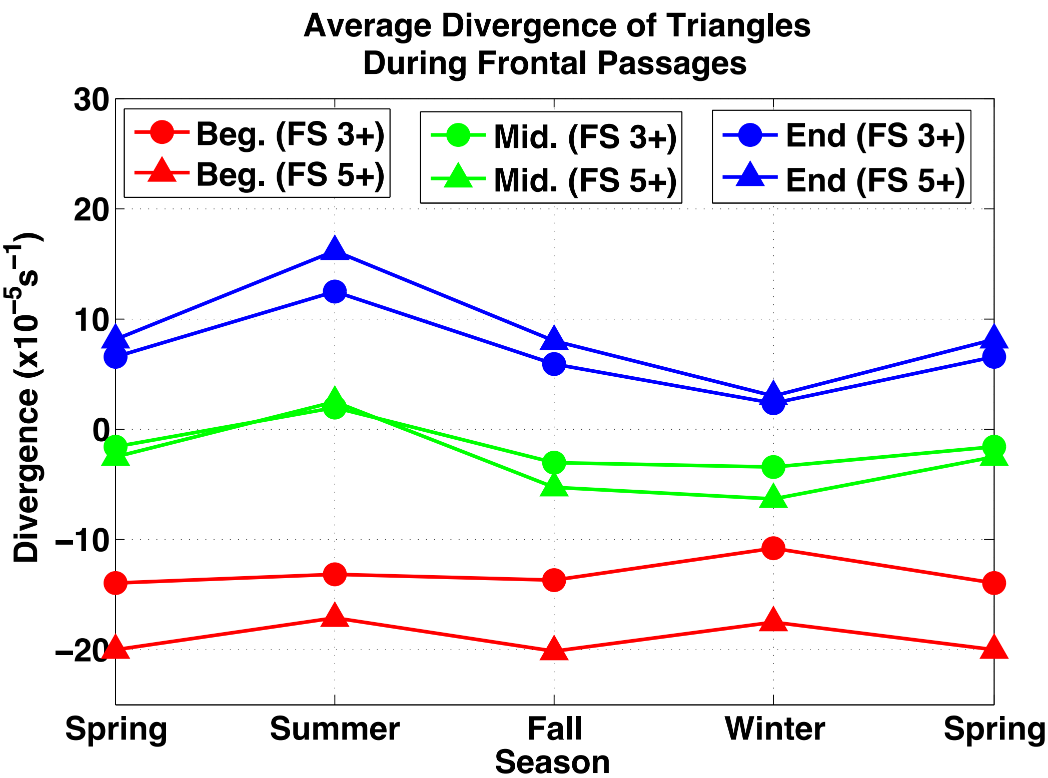

561 FIG. 6. Average divergence values (in $10^{-5}s^{-1}$) at the beginning, middle, and end of all (FS 3+) and strong
562 (FS 5+) frontal passages experienced by Mesonet triangles from 1997-2011 by season.

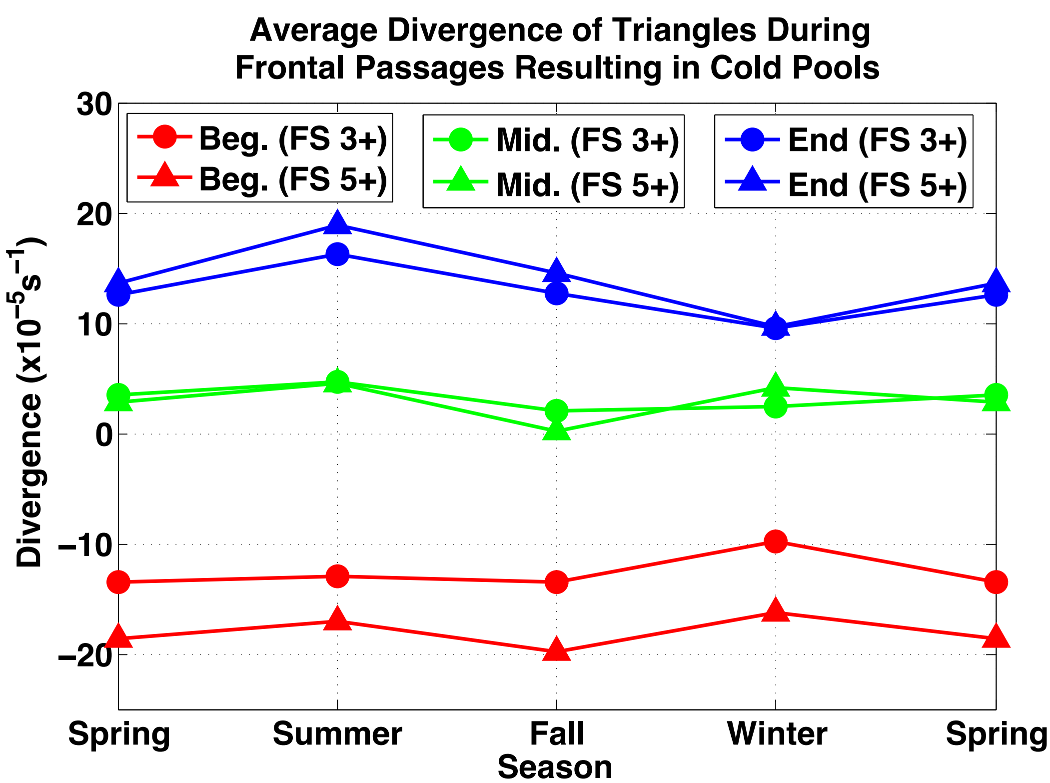

FIG. 7. Average divergence values (in $10^{-5}s^{-1}$) at the beginning, middle, and end of all (FS 3+) and strong (FS 5+) frontal passages resulting in cold pools experienced by Mesonet triangles from 1997-2011 by season.

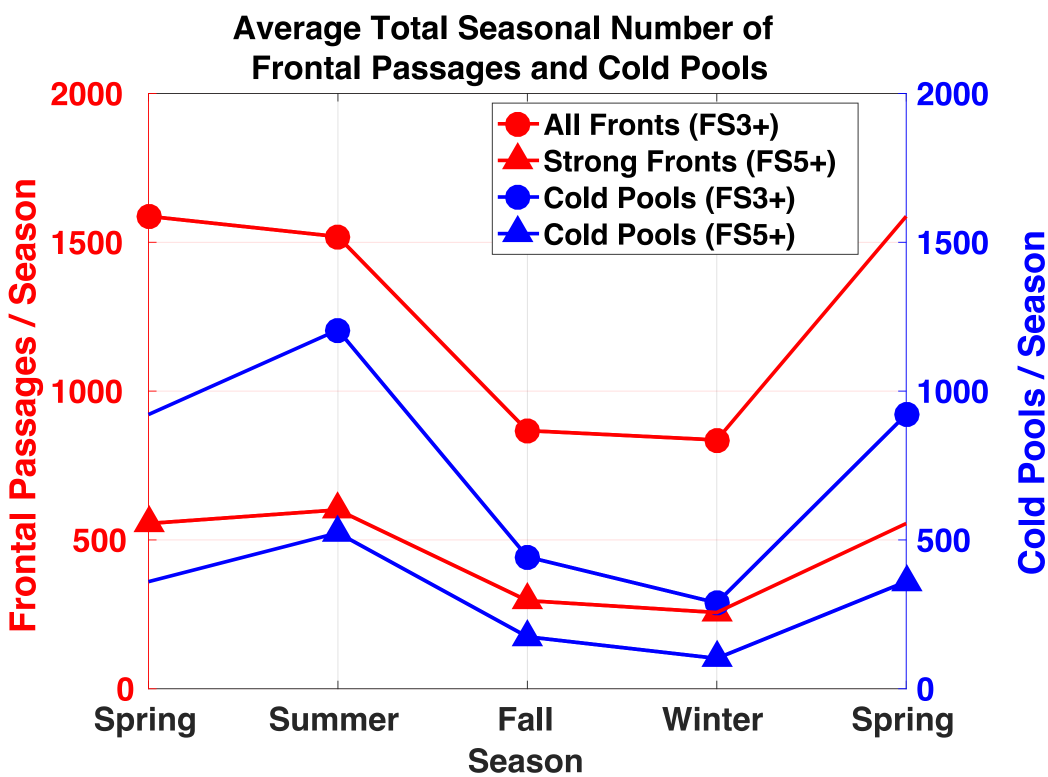

565 FIG. 8. Average total number of fronts (FS 3+), strong fronts (FS 5+), cold pools following all fronts (FS 3+),
566 and cold pools following strong fronts (FS 5+) experienced by Mesonet triangles per season from 1997 to 2011.

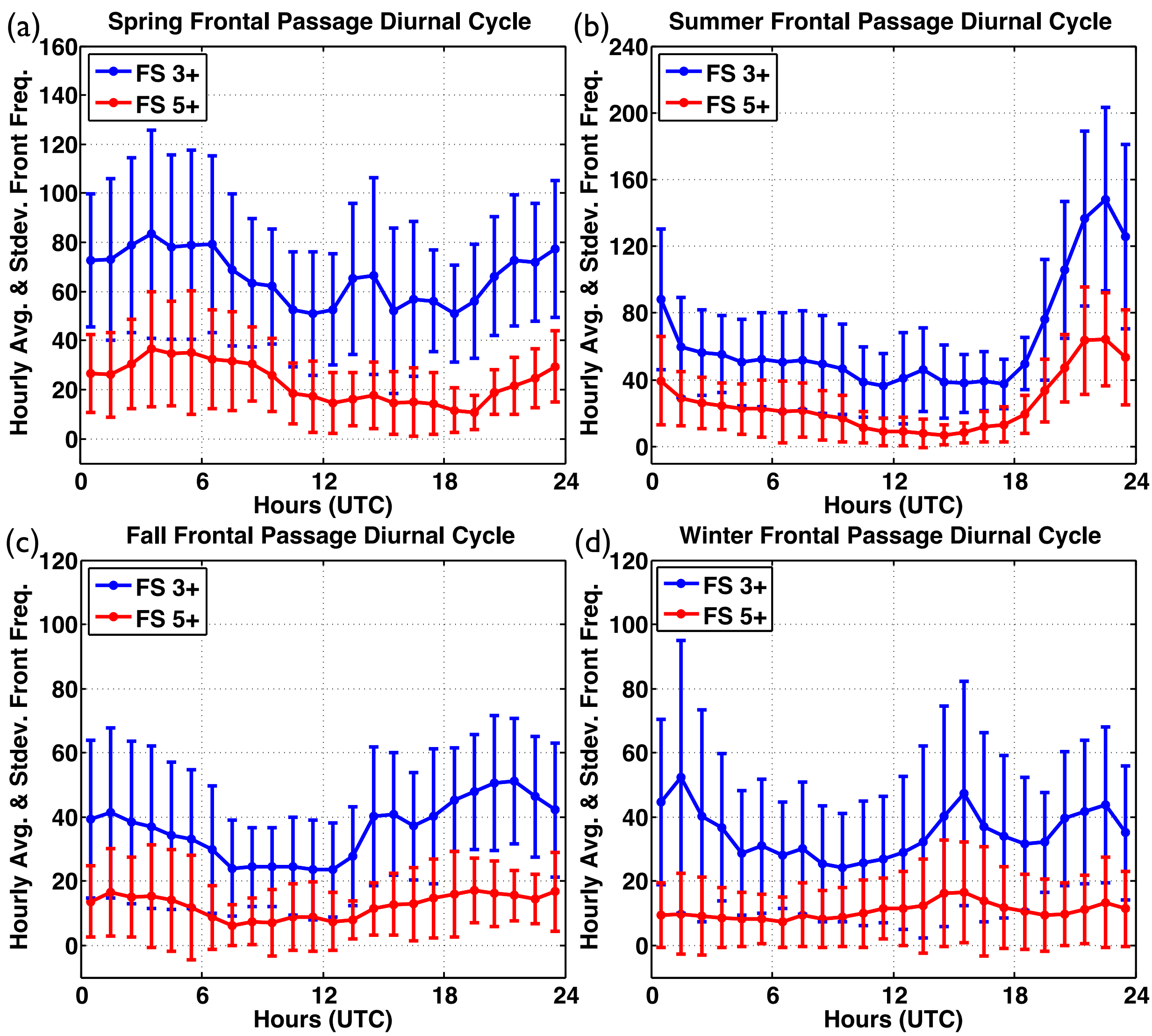

FIG. 9. Seasonally averaged diurnal cycle (in UTC time) of all (FS 3+) and strong (FS 5+) frontal passages at triangles in the Oklahoma Mesonet for the 1997-2011 period along with standard deviations. Results are shown for (a) spring, (b) summer, (c), fall, and (d) winter.

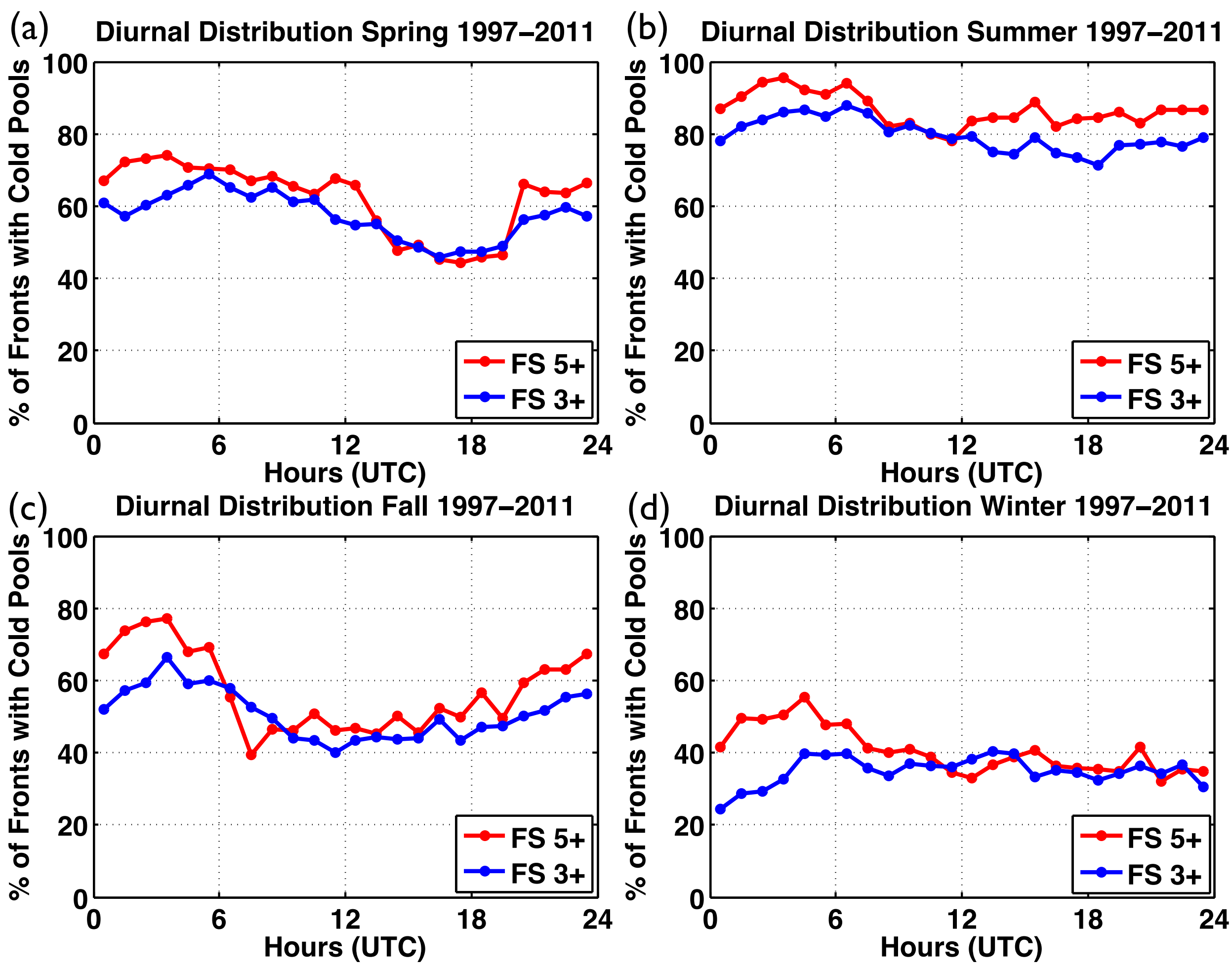

FIG. 10. Seasonally averaged diurnal cycle (in UTC time) of the percentage of all (FS 3+) and strong (FS 5+) fronts that yielded cold pools. Results are shown for (a) spring, (b) summer, (c), fall, and (d) winter.

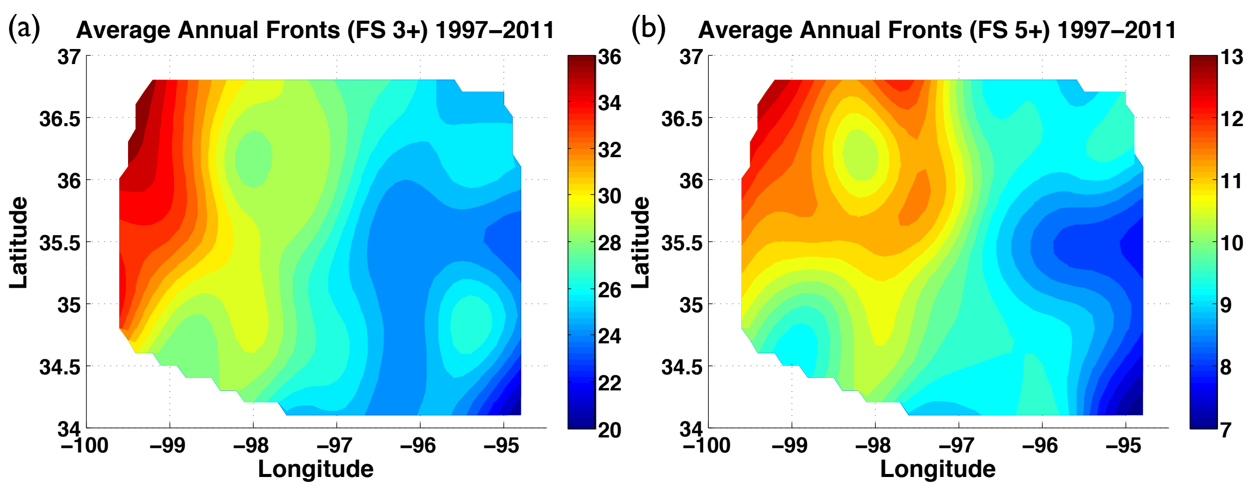

572 FIG. 11. Geographic distributions of (a) all frontal passages and (b) strong frontal passages. Frontal passage frequencies were adjusted using Mesonet triangle areas and longest side lengths, then spatially smoothed using a Barnes analysis.

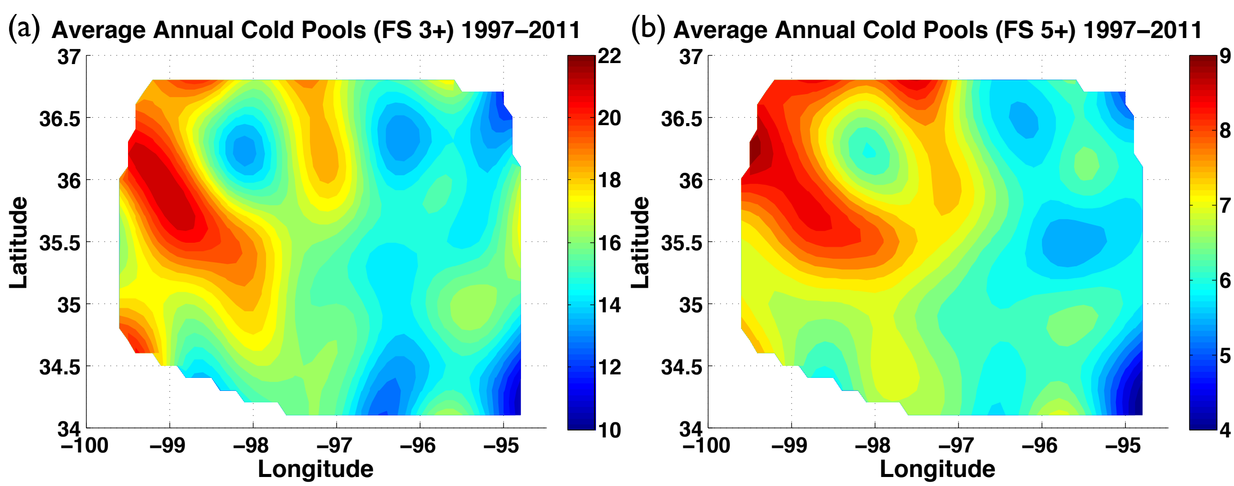

FIG. 12. Geographic distributions of (a) all cold pools and (b) cold pools following strong frontal passages. Cold pool frequencies were adjusted using Mesonet triangle areas and longest side lengths, then smoothed using a Barnes analysis.